




# Molecule–Electrode Electronic Coupling Modulates Optoelectronics of (Bio)Molecular Junctions

KUNCHANAPALLI RAMYA <sup>1,2</sup> and SABYASACHI MUKHOPADHYAY<sup>1</sup>

1.—Department of Physics, SRM University, AP, Guntur, AP 522503, India. 2.—e-mail: kunchanapalli\_ramya@srmmap.edu.in

The charge transport across a molecular junction formed by sandwiching molecules between two electrodes in testbed architectures depends not only on the work function of the metal electrodes and energy gap of the molecules but also on the efficacy of the molecule–electrode electronic coupling. Insights into such molecule–electrode coupling would help to understand the relation between the coupling strength and electron transport processes. With this aim, the optoelectronic modulation across bacteriorhodopsin-based molecular junctions has been studied using experimental current–voltage traces obtained by conducting-probe atomic force microscopy under various illuminations. The energy barrier ( $\varepsilon_0$ ), molecule–electrode coupling ( $\Gamma_g$ ), and other transport parameters were determined utilizing the Landauer model with a single-Lorentzian transmission function, transition voltage spectroscopy, and the law of corresponding states in the universal tunneling model approach. The findings reveal that the optoelectronic modulation of bacteriorhodopsin molecular junctions originate from alteration of the molecule–electrode coupling, which could originate from modulation of electronic states and the electrostatic environment of retinal chromophores made of the protein under dark and green or green–blue illumination conditions.

**Key words:** Biomaterials, molecular junctions, optoelectronics, electron transport

## INTRODUCTION

Bioelectronics is an emerging research discipline lying at the interface between biology and electronic science.<sup>1,2</sup> Over the years, bioelectronic devices have been developed focusing on the detection and analysis of biological signals utilizing electrical methods, but rarely involving the incorporation of biological materials into electronic devices. In the early 2000s, the introduction of solid-state electronic transport studies across protein monolayers utilizing nondestructive, soft-contact fabrication techniques and further electronic conduction studies at a single-biomolecule level with the scanning tunneling

microscopy technique opened the door to the incorporation of biomolecules as an active component in electronic devices.<sup>3</sup> The integration of photoactive biomolecules with manmade electrode surfaces has attracted great interest and holds significant promise from the perspective of bio(opto)electronics or energy capture interfaces.<sup>2,4</sup> In the work presented herein, we explored the potential of self-assembled bacteriorhodopsin (bR) protein monolayers as a chip-integrable optoelectronic material. Bacteriorhodopsin is a light-driven proton-pumping membrane protein with seven transmembrane helical structures, usually found in crystalline purple membrane patches (proteins embedded on lipid layers). Utilizing the photoactive retinal cofactor and proton transport channel, bacteriorhodopsin protein can convert absorbed light into chemical energy. Its dramatic light-induced structural effect,

(Received March 30, 2020; accepted June 9, 2020; published online June 24, 2020)

which leads to photoswitching and photochromism, suggests that bR could serve as an excellent biomaterial for constructing bio(opto)electronic devices for use in diverse technological areas, especially for the development and application of optogenetics.

Electronic transport (ETp) across wild-type and different variants of bR has already been studied in dry monolayer form, either in its native purple membrane environment or embedded in a partially delipidated membrane, and the nonlinear current–voltage ( $I$ – $V$ ) characteristic and photostimulated enhanced conduction upon green light illumination ( $\lambda > 500$  nm) have been reported.<sup>3,5,6</sup> Large-area measurements on purple membrane (PM) monolayers from which the lipids were partially removed (delipidated) confirmed that ETp occurs via the protein, rather than via the lipid layer in which the bR is embedded in the PM.

To enhance the electrical conduction across bR-containing monolayers and the corresponding optoelectronics modulation ratios at the nanoscale, we have explored partially lipid depleted WT-bR (delipidated bacteriorhodopsin, dLbR), where  $\sim 70\%$  of the lipids were removed from the PM with the aid of gentle detergent treatment. dLbR monolayers were prepared by immobilization on the surface of highly ordered pyrolytic graphite (HOPG) as a conducting substrate, taking advantage of the  $\pi$ – $\pi$  stacking interactions between the hydrophobic HOPG surface and the hydrophobic body of the protein that was previously buried inside the PM. Utilizing piezocontrol of the cantilever movement in conducting atomic force microscope, we developed an instantaneous (bio)molecular junction between the platinum-coated cantilever tip and monomeric dLbR on the conducting HOPG substrate (Fig. 1a). This HOPG–dLbR–Pt molecular junction configuration also allows us to acquire information on the ETp efficiency as a function of the tip force applied to the monolayer. Optoelectronic modulation of the monomeric dLbR monolayer was explored by accruing the  $I$ – $V$  characteristics of the dLbR molecular junctions under dark, followed by green ( $\lambda \approx 562$  nm) and

combined green–blue ( $\lambda \sim 562$  nm and  $\lambda \approx 405$  nm) illumination, similar to the photocycle of bR in its natural environment. In the case of bacteriorhodopsin films, the variation of the electrical conductance in the dark state and populated M-state under green illumination is directly related to the isomerization (*trans* to *cis*) process of the retinal chromophore, which alters the electronic configuration around the retinal pocket of the protein. In optoelectronic modulation of dLbR junctions, multiple successive measurements were carried out on a single dLbR junction, without withdrawing the tip, over illumination cycles with a period of 15–30 s. This results in modulation of the junction conductance that is typically reproducible over three full illumination cycles.

The photoisomerization of retinal chromophore leads to experimental variations in the measured current–voltage ( $I$ – $V$ ) characteristic even on the nanoscale with a few bR molecules ( $\sim 100$ , as estimated from its crystallographic structure dimensions), correlating the structure–function relationship of the biomolecule with its ETp efficiency in the molecular junction. Quantum-mechanical tunneling is the major transport mechanism in molecular electronics, but this cannot be generally described by a simple  $I$ – $V$  relation. In general, the ETp of molecular junctions depend on the highest occupied molecular orbital (HOMO)/lowest unoccupied molecular orbital (LUMO) levels of the molecule used, the Fermi energy levels of the metal electrodes ( $\varepsilon_L$ ,  $\varepsilon_R$ ), and the electronic coupling ( $\Gamma_L$ ,  $\Gamma_R$ ) between the molecular energy levels and metal electrodes (Fig. 1b). However, over the decades, many theoretical models have been formulated to produce simple, analytical  $I$ – $V$  relations, as described by the Simmons model, superexchange-mediated tunneling), or the Landauer model with a single-Lorentzian transmission function. While the resulting mathematical expressions are very different, they fit fairly well to the experimental  $I$ – $V$  trace, yielding different values for tunneling transport parameters such as the barrier height ( $\varepsilon_0$ ). In

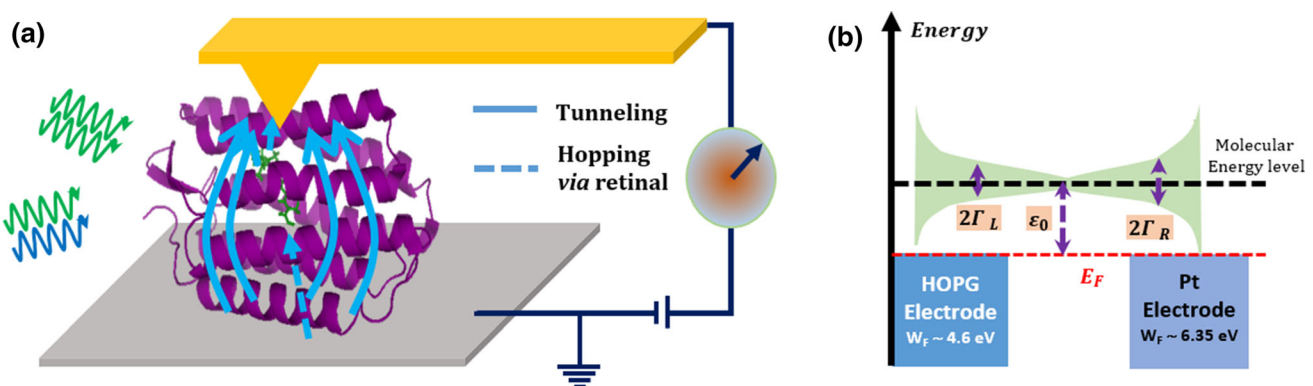


Fig. 1. (a) Schematic of (bio)molecular junctions between platinum-coated cantilever tip and monomeric dLbR on conducting HOPG substrate with possible electron transport pathways. (b) Schematic energy levels of dLbR-based molecular junctions with HOPG and Pt electrodes, showing that the intrinsic broadening of the molecular energy levels evolves via the molecule–electrode coupling.

the work presented herein, we analyzed  $I$ – $V$  traces obtained experimentally from optoelectronic modulation measurements on dLbR molecular junctions. We extracted tunneling parameters, mainly the energy offset/barrier height ( $\varepsilon_0$ ), conductance ( $G_{\text{eq}}$ ), and electronic coupling ( $\Gamma$ ), and used these to predict the origin of the optoelectronic modulations across dLbR molecular junctions in the dark and photoinduced M intermediate states.

## EXPERIMENTAL PROCEDURES

A freshly prepared dLbR monolayer on HOPG was characterized by noncontact-mode AFM imaging with minimal applied force (average < 500 pN) to confirm the formation of densely packed monolayers of dLbR protein from topographic images. Details of the preparation of the dLbR sample from PM solution and the monolayer formation process on the HOPG substrate are discussed in Ref. 7. Ultraviolet–visible (UV–Vis) absorption spectra of the monomer dLbR monolayers and multilayers revealed the characteristic absorption band of bR at  $\sim 560$  nm, suggesting that no major structure alteration occurred even in the dry delipidated monomeric configuration (see Supplementary Electronic Material Sect. S1 and Fig. S1). In electrical conduction measurements, the HOPG substrate was grounded and voltage was applied to the conducting tip, applying the AFM probe with a force of 4–7 nN to obtain stable  $I$ – $V$  traces with high signal-to-noise ratio and to avoid any change of the protein secondary structure. During ETp measurements, the electrical stability of each dLbR junction was first probed by scanning from 0.5 V to  $-0.5$  V at a rate of  $0.2 \text{ s}^{-1}$  (see Supplementary Material Sect. S6). At low voltages, the  $I$ – $V$  traces appeared linear (ohmic), but as the voltage was increased, they acquired an S-like shape, which was indifferent to the dark or light-adapted states of the dLbR molecules (Fig. 2a). This behavior was remarkably consistent considering the wealth of microscopic variables that affect the molecular transport, such as the energy alignment between the nearest molecular energy level and the Fermi levels of the metal contacts (barrier height,  $\varepsilon_0$ ), the transport distance dictated by the length of the molecule ( $L$ ), the coupling between the molecule and the contacts ( $\Gamma_L$ ,  $\Gamma_R$ ), and the coupling between the different molecular segments (amino acids and hydrogen bonds between tightly bound water molecules). The electrical quality of the junction was analyzed based on only the symmetric nature of the  $I$ – $V$  traces along the voltage axis. Around 50  $I$ – $V$  traces were acquired at a rate of  $0.2 \text{ s}^{-1}$  and statistically averaged for each junction. Finally, traces with less than 10% variation at  $\pm 0.5$  V were considered for further zero-bias ( $V_{\text{bias}} \leq \pm 100 \text{ mV}$ ) electrical conduction and electron transport analysis using MATLAB software.

The nonlinear  $I$ – $V$  behavior of the dLbR junction could be analyzed using a single-level transport model as widely applied in the context of molecular electronics with a single-level transmission function in the Landauer formula.<sup>8</sup> According to this model, the transport through a single-molecule junction is assumed to be dominated by elastic tunneling of electrons through a single molecular level of the energy barrier  $\varepsilon_0$  coupled to the left (L) and right (R) electrodes with a strength  $\Gamma_{L,R}$

$$I \cong N \frac{2e}{h} \Gamma_g^2 \frac{eV}{(\varepsilon_0 + \alpha eV)^2 - (\frac{eV}{2})^2} \text{ for } \Gamma_g = \sqrt{\Gamma_L \Gamma_R} \text{ and } \Gamma_g \ll \varepsilon_0, \quad (1)$$

where  $N$  is the number of molecules involved in the transport and  $\alpha$  is the asymmetric factor/voltage division factor, which is a dimensionless parameter with a value of  $\frac{1}{2}$  for a symmetric potential. The experimentally obtained  $I$ – $V$  traces for the dLbR junctions in dark and different types of illumination were analyzed using Eq. 1 to obtain the variations of  $\varepsilon_0$  and  $\Gamma_g$  between the dLbR and contact electrode under optoelectronic modulation. Details of the fitting methods and an example of an optoelectronic modulation set are presented in Supplementary Material Sect. S2.

Another approach that we applied to explain the origin of the optoelectronic modulation in dLbR junctions is the universal  $I$ – $V$  relation with a parabolic approximation, which suggests that the molecular conductance–voltage ( $G$ – $V$ ) trace should have a roughly parabolic shape (see Supplementary Material Sect. S3). In this approximation, the nonlinear tunneling current across any molecular junction ( $I$ ) is represented by a Taylor expansion of the applied bias voltage ( $V$ )

$$I = G_{\text{eq}} V \left[ 1 + S \frac{V}{V_0} + \left( \frac{V}{V_0} \right)^2 \right], \quad (2)$$

where  $G_{\text{eq}}$ ,  $V_0$  and  $S$  are the equilibrium conductance, scaling voltage, and asymmetry factor, respectively. Differentiating Eq. 2 to obtain the differential conductance yields

$$\frac{dI}{dV} = G(V) = G_{\text{eq}} \left[ 1 + 2S \frac{V}{V_0} + 3 \left( \frac{V}{V_0} \right)^2 \right]. \quad (3)$$

Physically, the equilibrium conductance is the value of the conductance at zero bias, which is directly proportional to the number of molecules ( $N$ ) and exponentially inversely proportional to the molecular length or tunneling distance ( $L$ ) given by

$$G_{\text{eq}} = G(0V)N \cdot e^{-\beta L}. \quad (4)$$

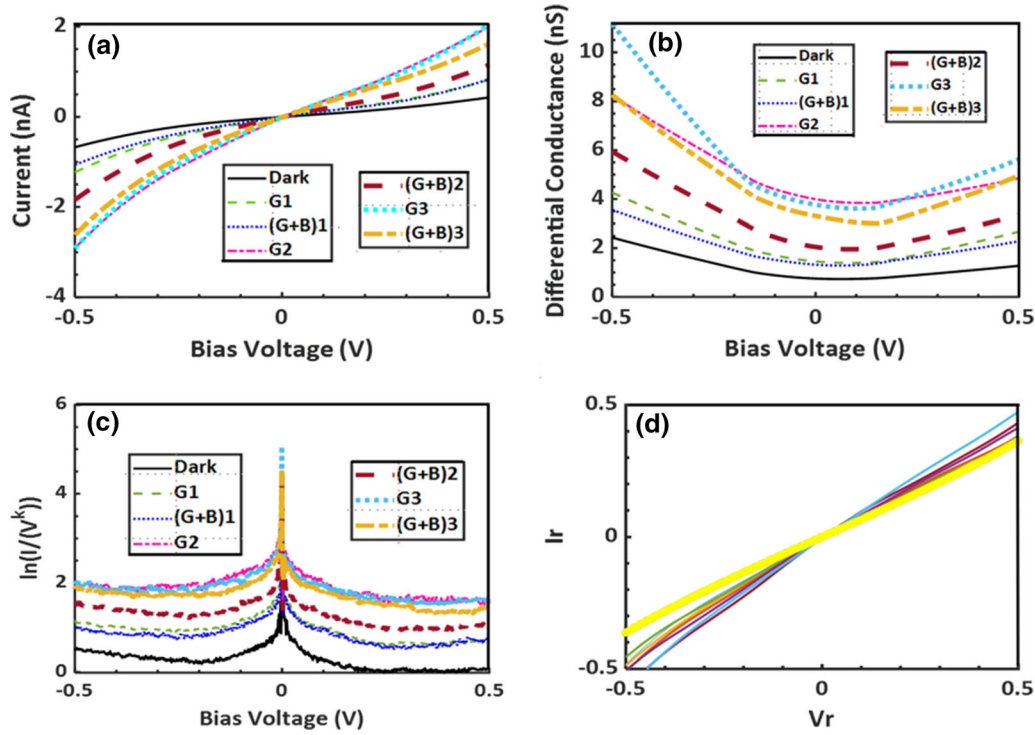


Fig. 2. (a) Example of optical modulation  $I$ - $V$  sets obtained with dLbR molecular junction, analyzed using the (b) differential conductance and (c) normalized differential conductance method. (d) Representation of universal curves with theoretical LCS (yellow, thick line) under dark conditions and various types of illumination (thin lines) (Color figure online).

The scaling voltage refers to phase transitions that are not related to the tunneling but depends on the energy offset  $\varepsilon_0$ . The asymmetry factor is very small, arising due to the asymmetric tunneling considering the applied bias, i.e., in the case of an asymmetric potential across the junction, which we expect to originate from the different work functions of the electrodes (HOPG and Pt) used here (Fig. 1b). The polynomial coefficients in the Taylor expansion presented above were computed from the value near to zero bias utilizing the first and second numerical derivatives of experimental conductance traces (see Supplementary Fig. S3). The variations of these coefficients were further analyzed to reveal the origin of the modulated electronic transport across the dLbR molecular junction under dark and illuminated cycle conditions along with different forces applied on the dLbR monolayer by the AFM probe.

The tunneling current across the dLbR junction is nearly linear in the applied voltage in the zero-bias regime, but behaves nonlinearly at certain applied voltages where a transition from simple tunneling to field emission occurs, which is defined as the transition voltage ( $V_t$ ). We analyzed our experimentally obtained dLbR optoelectronic modulated  $I$ - $V$  traces using the tunneling model proposed by Fowler and Nordheim. The transport model was developed for inorganic potential barriers, where there is a transition from a trapezoidal-shaped potential (normal tunneling) to a triangular potential (field emission) when the bias voltage exceeds

the energy offset of an insulator junction.<sup>9,10</sup> The transition voltage is nothing but the mathematical minimum of the Fowler–Nordheim (FN) function, i.e.,  $\ln(\frac{I}{V^k})$  in Fowler–Nordheim plots showing  $\ln(\frac{I}{V^k})$  versus  $V$ . The plots exhibit logarithmic growth in the low-bias regime. In experimental conditions, when the applied bias is near the barrier height, field emission dominates, causing a transition from logarithmic growth to linear decay. This transition corresponds to the transition voltage  $V_t$ . The significant feature of this method is that it properly accounts for the asymmetric potential profile in the dLbR junction with HOPG and Pt-coated AFM probes as electrodes. We plot the experimental  $I$ - $V$  traces of the dLbR junction as  $\ln(\frac{I}{V^k})$  versus  $V$  in Fig. 2c and obtain the transition voltage  $V_t$  by finding the mathematical minimum of the function  $\ln(\frac{I}{V^k})$  by imposing the condition

$\frac{\partial(\frac{I}{V^k})}{\partial(V)} = 0$ . Transport parameters such as  $\varepsilon_0$ ,  $\alpha$ , and  $G_{eq}$  were extracted based on Simmons's transport model for each experimental  $I$ - $V$  trace, utilizing the corresponding transition voltages (Fig. S4b).

$$\varepsilon_0 = \frac{q\Pi}{\sqrt{\Sigma^2 + \Pi \cdot \frac{4}{(1-k^{-2})}}}, \quad (5)$$

where the asymmetry factor is



$$\alpha = \frac{\Sigma}{2\sqrt{\Sigma^2 + 4\Pi}} \quad (6)$$

and

$$G_{\text{eq}} = \frac{I_t}{V_t} \left( 1 + 2\alpha \frac{qV_t}{\varepsilon_0} - (0.25 - \alpha^2) \left( \frac{qV_t}{\varepsilon_0} \right)^2 \right). \quad (7)$$

Due to the electrode work function asymmetry in the dLbR junction, the FN plots also become asymmetric, as reflected in the different magnitudes of the transition voltage  $V_{k+} \neq -V_{k-}$  for each bias polarity ( $V < 0$  or  $V > 0$ ), where  $\Pi$  and  $\Sigma$  are expressed as  $\Sigma = V_k^+ + V_k^-$  and  $\Pi = |V_k^+ \cdot V_k^-|$ .

Finding the accurate transition voltage for a junction with an asymmetric potential is not trivial, and the extraction of the transport parameters largely depends on how accurately the transition voltage can be found by fitting to experimental data. To eliminate error in finding the accurate minimum of the Fowler–Nordheim function used in transition voltage spectroscopy as discussed earlier, we further normalized our conductance data following the normalized differential conductance (NDC) method (see Supplementary Material Sect. S4 and Fig. S4a, b). Mathematically, the NDC is nothing but the ratio of the differential conductance to the conductance or the derivative of  $\frac{\ln(I)}{\ln(V)}$ , which is given by  $\text{NDC} = \frac{dI}{dV} \frac{V}{I}$ .

Combining the parabolic approximation for the tunneling current with the NDC, one obtains

$$\text{NDC} = G(V) \frac{V}{I} = \frac{1 + 2S \frac{V}{V_0} + 3\left(\frac{V}{V_0}\right)^2}{1 + S \frac{V}{V_0} + \left(\frac{V}{V_0}\right)^2}. \quad (8)$$

By setting  $\text{NDC} = k$  in Eq. 8, the scaling voltage and asymmetry factor can be expressed as

$$V_0^2 = \left| V_{t,k}^+ \cdot V_{t,k}^- \right| \cdot \frac{3-k}{k-1} \quad \text{and} \quad (9)$$

$$S = - \left[ \frac{\left( V_{t,k}^+ + V_{t,k}^- \right)}{V_0} \right] \cdot \left[ \frac{(3-k)}{(2-k)} \right].$$

Utilizing the above equations, we extracted the scaling voltage, the asymmetry factor, and the accurate value of  $k$  where the transition exactly occurs for the dLbR molecular junction during optoelectronic modulation applied on the dLbR using AFM probes.

Insights into the ETp across different molecular junctions were obtained based on the conductance–voltage characteristic, transition voltage spectroscopy, normalized differential conductance, and single-level transmission function using the Landauer formula. All the analytical models enable us

to extract the energy offset ( $\varepsilon_0$ ), asymmetry factor, and electronic coupling strengths under the mentioned assumptions adopted during their development. Therefore, finding a suitable tunneling model for a specific type of molecular junction is crucial for understanding the relationship between the chemical details of the contact–molecule–contact system and its electrical performance, where the prior assumptions fit well with the design of the specific molecular junction considered. We extended our studies to the  $I$ – $V$  traces obtained from dLbR molecular junctions for dLbR optoelectronic modulations.

## RESULTS AND DISCUSSION

We assumed that tunneling is the dominant mechanism in the electron transport process across the dLbR molecular junctions. To provide further support, we analyzed the experimentally obtained  $I$ – $V$  traces of dLbR junctions using different tunneling transport models along with the law of corresponding states (LCS), which has been applied to represent the electron transport across molecular junctions in a universal manner (Fig. 2d). The LCS provides a series of equilibrium properties describing the charge transport across a molecular junction in the regime where the tunneling current is linear in the applied bias. LCS analysis was specifically developed for electron tunneling, as a unified theoretical model to describe the tunneling phenomenon with a universal curve that characterizes the experimental transport behavior of molecular junctions. The LCS is expressed by a universal  $I$ – $V$  curve that is free of empirical parameters and unaffected by stochastic fluctuations of the electron transport in molecular junctions.

The LCS analysis starts from the universal van der Waals equation of state for real gases, which predicts that all fluids behave similarly at equilibrium. The critical values of pressure ( $P_C$ ), volume ( $V_C$ ), and temperature ( $T_C$ ) are used to prove the universality of gases at equilibrium in terms of reduced parameters that obey the equation  $\left( p_r + \frac{3}{V_r^2} \right) \left( V_r - \frac{1}{3} \right) = \frac{8}{3} T_r$ , where  $P_r$ ,  $V_r$ , and  $T_r$  are the reduced parameters given in terms of the critical parameters as  $P_r = \frac{P}{P_C}$ ,  $V_r = \frac{V}{V_C}$ , and  $T_r = \frac{T}{T_C}$ . Similarly, the tunneling transport across molecular junction can be analyzed using the law of corresponding states based on experimental  $I$ – $V$  traces with the critical values of the bias voltage ( $V_C$ ) and current ( $I_C$ ). Figure 2a presents a set of optoelectronic modulations in the dLbR junction under various illumination conditions in a successive manner. Figure 2d presents a universal LCS curve expressing the current and applied bias in terms of the reduced quantities  $V_r$  and  $I_r$ . The reduced voltage  $V_r = \frac{V}{V_C}$  and current  $I_r = \frac{I}{I_C}$  can be deduced from each experimental  $I$ – $V$  traces, after obtaining the critical current ( $I_C$ ) and critical voltage ( $V_C$ )

values for each individual  $I$ - $V$  trace (see Supplementary Material Sect. S5). The critical voltage  $V_C$  values of the individual  $I$ - $V$  datasets are found as the maxima of the curves obtained by plotting  $|V^2/I|$  versus  $V$ , where  $V$  is the bias voltage and  $I$  is the junction current which represents the transition from tunneling to field emission, characterized by the crossover between the linear and nonlinear regime of the current versus applied bias. The critical current ( $I_C$ ) values for the individual  $I$ - $V$  traces were found as the corresponding value of current at the transition voltage  $V_C$  in the plot of abs. current versus bias voltage (see Supplementary Material Sect. S5 and Fig. S5).

The reduced current-voltage characteristic provides a new parameter-free transport equation as  $I_r = \frac{2V_r}{3-V_r^2}$ , which is shown by the yellow line in Fig. 2d. The reduced transport graph coincides with the individual reduced  $I$ - $V$  traces near to zero voltage but deviates at higher applied bias. This can be attributed to the temperature-related retinal vibration, which contributes to hopping transport paths across the dLbR junction at high bias. Our LCS analysis of the  $I$ - $V$  traces in Fig. 2d validates the theory of the unified law of corresponding states for tunneling transport across dLbR-based molecular junctions. The transport parameters such as the energy barrier and zero-bias conductance were evaluated based on the critical values of the voltage and the corresponding current ( $eV_c = \frac{2\varepsilon_0}{\sqrt{3}}$  and  $I_c = \frac{G\varepsilon_0\sqrt{3}}{e}$ ) for individual  $I$ - $V$  traces in both the positive and negative bias regimes, as listed in the comparison tables in the Supporting Information.

In the differential conductance approach, the numerically computed conductance  $\frac{dI}{dV}$  versus  $V$  is obtained from the  $I$ - $V$  traces based on the polynomial relation in Eq. 3. Transport parameters such as the scaling voltage and asymmetric parameters can be found for each  $I$ - $V$  trace under dark and various illumination cycles, as summarized in Supplementary Tables SI-SV.

Similarly, transport parameters such as the energy barrier, asymmetry factor, and equilibrium conductance can also be obtained from the optoelectronic modulated  $I$ - $V$  traces utilizing transition voltage ( $V_t$ ) and NDC analysis, following Eqs. 6, 7, and 8. Because of the asymmetric nature of dLbR molecular junctions, we first found  $k$  (the factor of quality of tunneling) for the individual traces using the NDC method i.e.  $\frac{dI}{dV}$  versus  $V$  plot (Supplementary Fig. S4a). The transition voltage ( $V_t$ ) at which the transition from tunneling to field emission occurs was found by plotting  $\ln\left(\frac{I}{V^k}\right)$  versus  $V$  individually (see Supplementary Fig. S4b). Since we utilized an average of  $\sim 50$  experimental  $I$ - $V$  traces, the smoothing factor

played an important role in our NDC analysis. Depending on the shape of the plot, the smoothing factor varies under various conditions such as dark and different types of illumination. We restricted the analysis to different smoothing factors for each  $I$ - $V$  trace with minimum deviations (Supplementary Fig. S4a, b). The experimental  $I$ - $V$  traces obtained from dLbR molecular junction in the dark and under various types of illumination were fit using a single-level transport model, i.e., Landauer approach, and the energy offset ( $\varepsilon_0$ ), asymmetry factor ( $\alpha$ ), and coupling strength ( $\Gamma_g$ ) between the molecules and electrodes were computed from the fitting parameters.

Figure 3a summarizes the conductance modulation of the dLbR molecular junction in the dark state and under green and green + blue illumination in successive cycles as computed using the parabolic approximation (GV), transition voltage spectroscopy (TVS), and law of corresponding state (LCS) analysis, where  $G_{\text{green}} > G_{\text{green+blue}} > G_{\text{dark}}$ .

These findings suggest that green illumination indeed excites the retinal chromophore in dLbR monomers and that the resulting enhancement in the junction conductance could be associated with the formation and accumulation of the photochemically induced M-like dLbR intermediate (absorbing at around 410 nm) (Fig. 3a). The modulation of the conductance with successive cycles rules out junction heating upon illumination as the cause of the conductance changes. Additional blue light with

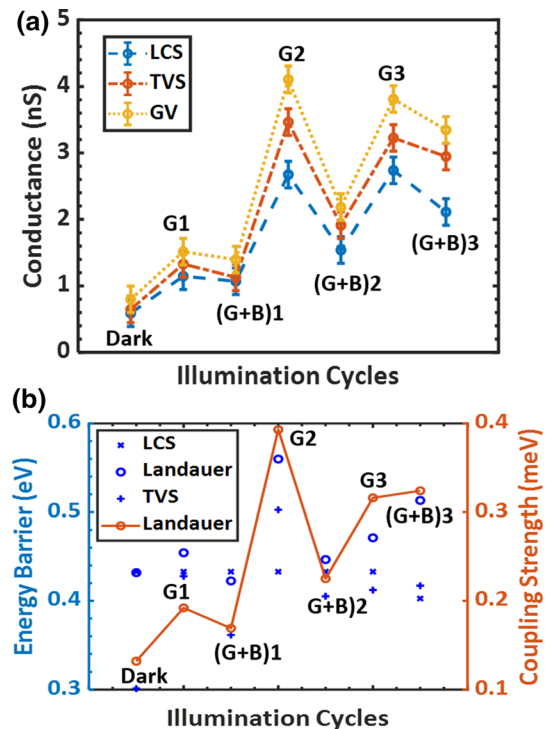


Fig. 3. (a) Conductance variation of dLbR molecular junction under optical modulation as obtained from calculation. (b) Variation of computed energy barrier and coupling strength of dLbR junction during an optoelectronic modulation cycle.

green illumination decreases the junction conductance, as the blue light mainly excites the M-like intermediate, accelerates its conversion back to the initial dark dLbR state by shortening its lifetime, and thus decreases its fraction in the mixture of the M-like intermediate and ground (dark) state.

Earlier, optoelectronic modulation findings on PM monolayers in macroscopic junctions and also with conducting-probe atomic force microscopy (CP-AFM) measurements (with an applied tip force of 12 nN to 15 nN) in the dark and under green illumination inducing the M-like state were explained based on the stronger H-bonding network in the M-state than in the dark dLbR state, which may lower the activation energy for transport. Interestingly, when we analyzed the experimental  $I$ - $V$  traces using transport models, the variation of the computed energy offset or barrier ( $\epsilon_0$ ) for the dLbR molecular junctions lay within  $\leq 50$  meV with illumination modulations. Obvious correlations between the modulated conductance of the dLbR junction and the corresponding energy offset were not found from our calculations (Fig. 3b), whereas the variation in the computed coupling strength  $\Gamma_g$  exactly replicated the junction conductance modulation profiles as examined over  $\sim 30$  junctions (Fig. 3a, error bars show the variation among junctions).

In dLbR, tightly bound water molecules in the retinal pocket bridge two negative moieties D85 and D212 of the retinal Schiff base through hydrogen bonding. These two negative moieties and the bridging water molecule form a pentagonal hydrogen-bonding network. These water molecules are involved in the light-induced protonation process and retinal photoisomerization. Molecular dynamics simulations [utilizing the *ab initio* multiple spawning (AIMS) method] of light-induced retinal (in the form of charge) modified protonated Schiff base with complex counterion supported that the positions of the D85 and D212 residues as well as the hydrogen-bonding network at the retinal binding site remain as close as possible in the native dark state, but are reorganized in the excited state dynamics.<sup>11–13</sup> Analysis of the methylated, long-carbon-chain (up to unreduced) retinal models suggests a two-state, two-mode mechanism for the retinal photoisomerization process, where two modes (first skeletal deformations then torsions about the reacting double bond) characterize the molecular motion along the photoisomerization path and two states are involved in the photoinduced wave packet dynamics.<sup>13,14</sup> Thus, the retinal photochemistry plays a crucial role in determining the environmental electrostatics of the retinal pockets. The different (covalent or ionic) electrostatic nature of the dark ground states and light-induced excited states determines the different energy landscape of those states, regulated by the overall photoisomerization mechanism, photochemical efficiency, and reaction selectivity.

The results of our theoretical analysis of the experimental optoelectronic modulation ( $I$ - $V$  traces) are in good agreement with the molecular dynamics simulation of the retinal chemosphere and its interaction with electrodes. In solid-state electron transport across dLbR monolayers, retinal plays a crucial role, and the nature of its electronic states and electrostatic environment determines the overall electronic coupling of dLbR-based molecular junctions. The ionic nature of the protonated Schiff base in the light-induced M-state enhances the electronic coupling of the HOPG–retinal–metal junction, which manifests as efficient transport, i.e., higher current at given bias in comparison with dark states.

## CONCLUSIONS

We explored the potential of monomeric bR as an efficient optoelectronic material by extracting it from its membrane environment. Under an applied force of 10 nN (via the CP-AFM probe), dLbR molecular junctions were stable within the  $\pm 1$  V bias regime with current  $< \pm 10$  nA, at room temperature and in a controlled atmosphere (4% to 20% RH,  $N_2$  environment). It was also observed that large-area (with  $\sim 10^{10}$  mol) biomolecular junctions were stable even at low temperatures ( $\sim 80$  K), where the sudden decline of the junction current observed above 320 K may originate from biological decomposition.<sup>15</sup> To demonstrate the practical viability of nanoscopic biomolecular junctions using 10 to  $10^2$  molecules as probes, their temperature-dependent transport and junction stability must be explored. In summary, in a molecular junction, the dLbR monomer in its photoinduced intermediate M-like state is a more efficient electron transport medium than in its dark-adapted ground state. The efficiency of electronic transport is dominated by the electronic states and electrostatic environment of retinal resulting from the charge distribution over the protonated Schiff base. We suggest that alteration of the electrostatic environment facilitates the variation of the electronic coupling between retinal and electrodes, which manifests as optoelectronic modulation of the dLbR junction. In conclusion, we explored different transport models to analyze the optoelectronic modulation of dLbR molecular junctions. The findings provide fundamental insights into the optoelectronic properties of dLbR junctions, which can be considered as a photoswitchable biomaterial for solid-state current-carrying electronic elements to integrate with bioelectronic device structures.

## ACKNOWLEDGMENTS

K.R. acknowledges financial support from the Department of Physics, and SRM University research program for her doctoral fellowship. S.M. acknowledges SERB-DST, Govt. of India for Early Career Research Award Grants (ECR/2017/001937),

and SRM University research funding for financial support. We acknowledge support from the Chemical Research Support group of WIS, Israel for experimental facilities and scientific discussions.

### ELECTRONIC SUPPLEMENTARY MATERIAL

The online version of this article (<https://doi.org/10.1007/s11664-020-08263-y>) contains supplementary material, which is available to authorized users.

### REFERENCES

1. S.S. Panda, H.E. Katz, and J.D. Tovar, *Chem. Soc. Rev.* 47, 3640 (2018).
2. J.J. Davis, D.A. Morgan, C.L. Wrathmell, D.N. Axford, J. Zhao, and N. Wang, *J. Mater. Chem.* 15, 2160 (2005).
3. I. Ron, L. Sepunaru, S. Itzhakov, T. Belenkova, N. Friedman, I. Pecht, M. Sheves, and D. Cahen, *J. Am. Chem. Soc.* 132, 4131 (2010).
4. O. Berthoumieu, A.V. Patil, W. Xi, L. Aslimovska, J.J. Davis, and A. Watts, *Nano Lett.* 12, 899 (2012).
5. A.V. Patil, T. Premaruban, O. Berthoumieu, A. Watts, and J.J. Davis, *J. Phys. Chem. B* 116, 683 (2012).
6. Y.D. Jin, N. Friedman, M. Sheves, and D. Cahen, *Adv. Funct. Mater.* 17, 1417 (2007).
7. A.V. Patil, T. Premaruban, O. Berthoumieu, A. Watts, and J.J. Davis, *Chem. Eur. J.* 18, 5632 (2012).
8. T. Ando, *Mesoscopic Physics and Electronics*, ed. T. Ando, Y. Arakawa, K. Furuya, S. Komiyama, and H. Nakashima (Berlin: Springer, 1998), pp. 11–14.
9. A. Vilan, *J. Phys. Chem. C* 111, 4431 (2007).
10. A. Vilan, D. Cahen, and E. Kraisler, *ACS Nano* 7, 695 (2013).
11. M. Ben-Nun, J. Quenneville, and T.J. Martínez, *J. Phys. Chem. A* 104, 5161 (2000).
12. C. Punwong, T.J. Martínez, and S. Hannongbua, *Chem. Phys. Lett.* 610–611, 213 (2014).
13. E. Nango, et al., *Science* 354, 1552 (2016).
14. J. Allen, *F1000 Fac. Rev. Res.* 8, 211 (2019).
15. L. Sepunaru, N. Friedman, I. Pecht, M. Sheves, and D. Cahen, *J. Am. Chem. Soc.* 134, 4169 (2012).

**Publisher's Note** Springer Nature remains neutral with regard to jurisdictional claims in published maps and institutional affiliations.